Continuous microflow synthesis of fluorescent phosphorus and nitrogen co-doped carbon quantum dots

Liangliang Lin[1,2*], Yijian Yin[3], Ziyang Li[1], Hujun Xu[1], Volker Hessel[4], Kostya (Ken) Ostrikov[5]

[1] School of Chemical and Material Engineering, Jiangnan University, Wuxi 214122, China

[2] Key Laboratory of Nanodevices of Jiangsu Province, Suzhou 215123, China

[3] College of Chemical and Biological Engineering, Zhejiang University, Hangzhou 310027, China

[4] School of Chemical Engineering and Advanced Materials, The University of Adelaide, North Terrace Campus, Adelaide 5005, Australia

[5] School of Chemistry and Physics and QUT Centre for Materials Science, Queensland University of Technology (QUT), Brisbane, QLD 4000, Australia.

*Corresponding authors: linliangliang@jiangnan.edu.cn;

Abstract: Fluorescent carbon quantum dots (CQDs) doped with heteroatoms are highly promising for diverse applications ranging from bioimaging to environmental sensing. However, the ability for doping and functionalizing CQDs in a continuous, scalable, industry-relevant flow chemistry process, remains limited. Here we overcome this limitation by developing a continuous, facile and efficient method for the preparation of nitrogen and phosphorus co-doped carbon quantum dots (NP-CQDs), using microflow reactors combined with localized, energy-efficient heating of ethanolamine and phosphoric acid aqueous solution. The products are characterized by advanced microanalysis including fluorescence spectrophotometry, transmission electron microscopy, X-ray photoelectron spectroscopy, and X-ray diffraction (XRD)

measurements. The results show ultrasmall fluorescent CQDs with narrow size distribution were successfully prepared, where N and P atoms proved to be effectively doped into the CQDs. The reaction conditions for the continuous synthesis of CQDs are investigated, including the influence of residence time and reaction temperature on the obtained CQDs (particle size, distributions, fluorescence intensity, and fluorescence lifetime) are analyzed). This study is expect to provide a guidance for the continuous and controllable preparation of fluorescent CQDs with effective doping of heteroatoms.

Keywords: microreactor; microchannels; process intensification; carbon quantum dots; continuous synthesis

Highlight:

- A microflow technique is applied for N/P co-doped carbon quantum dots synthesis.
- The continuous microflow approach is effective for the co-doping of heteroatoms.
- The properties of the co-doped carbon dots can be controlled by process parameters.
- The photoluminescence performance of the carbon dots were further evaluated.

1. Introduction

In the past two decades, the development of functional nanomaterials has witnessed rapid acceleration and expansion. Nanomaterials, as suitable biomedical, energy, and environment materials, have attracted strong attention from academy and industry (Ma et al., 2019). Due to their unique physical and chemical properties, they are actively explored for applications in nanotechnology and chemical engineering. In last decades, fluorescent nanomaterials were found capable of visualizing and imaging the evolution of biological processes at the cellular or subcellular level, making them a versatile tool in bio-applications (Lin et al., 2019). Among them, carbon quantum dots (CQDs) have key benefits of low toxicity, good water solubility and chemical stability, strong fluorescence, as well as the low cost. These features, along with excellent biocompatibility has endowed CQDs with many merits that are desirable in biomedical applications, such as drug delivery, disease diagnosis, bio-sensing, and imaging-guided therapy.

The electrochemical and optical properties of CQDs can be dramatically enhanced by doping heteroatoms. For instance, nitrogen doping proved to be an effective strategy to overcome the inherent low quantum yields of conventional CQDs. The introduction of dopant atoms like N, S, O, P, etc. into CQDs can create different emission centers and traps, as well as can modify the electronic structures of CQDs. As a consequence, their emission spectra can be flexibly tuned to a large extent (Ma et al., 2020). Recently, it has been reported that the co-doping CQDs, such as N, S co-doping (NS-CQDs); N, B co-doping (NB-CQDs); N, P co-doping (NP-CQDs), etc., can be used to achieve

better optical and electrochemical properties compared with the single-element doping. This is due to the synergistic effect of different heteroatoms (Li et al., 2019). CQDs co-doped with multi-elements also possess abundant functional groups (e.g. -OH, -COOH, -SH, $-NH_2$, and $-PO_3$, etc.) on their surface, endowing them with extra functionalities by conjugation with functional molecules or polymers, which can further extend their application range (Park et al., 2016). Thus, doping/co-doping of heteroatoms in CQDs becomes a robust and versatile way to further improve the chemical composition and properties of CQDs.

Currently, several methods have been developed to synthesize fluorescent CQDs. Castro et al. (Castro et al., 2016) reported a laser ablation method to prepare ultra-small CQDs (1.5 - 3.0 nm) in ionic liquids media, where CQDs can be stabilized by an electrostatic layer of ionic liquids. As a result, the fluorescence emission of CQDs becomes much broadened due to the altered electrostatic potential. Ling et al. (Ling et al., 2020) developed a magnetic heating method for rapid, single-step synthesis of excitation-dependent fluorescent CQDs, which were further used as ink for inkjet printing to produce fluorescent patterns. In a recent study, N-CQDs of stable fluorescence, excellent cell permeability, and high photothermal conversion efficiency (42.4%) were produced via a hydrothermal method. By converting sunlight to heat, the as-prepared N-CQDs also showed intrinsic anti-cancer and anti-fungal activities. Zhang et al. (Qu et al., 2020) demonstrated the construction of a dual-mode colorimetric/ratiometric fluorescent probe using N-CQDs, which were successfully applied for highly sensitive and selective detection of formaldehyde in living cells.

Despite the significant progress in the synthesis and application of heteroatom-doped CQDs, several major limitations still exist. Traditional methods rely on labor- and energy-consuming selection of reagents and experimental conditions, so the synthesis of high performance CQDs or CQDs with targeted dopant atoms is often a tedious and time-consuming work. There are also many factors affecting the fluorescence performance of CQDs, such as carbon precursors, reaction time, solvents, dopants, surface functional groups, and particle size. However, there are no exhaustive guiding principles for the synthesis of CQDs with customized properties. The situation becomes even more complex for CQDs with multi-element doping. Thus, the ability for precise CQDs synthesis and engineering, especially in a continuous, scalable, industry-relevant flow chemistry processes, remains essentially limited. Furthermore, the emission mechanism of CQDs in many cases still remain unclear. Consequently, the controllable preparation of fluorescent CQDs and the study of the fluorescence mechanisms are crucial for practical applications of CQDs (El-Shabasy et al., 2021).

Compared with conventional batch reactors, microreactors have the advantages of high surface area to volume ratio, high efficiency of heat and mass transfer, good reaction reproducibility, as well as feasibility for industrial scale-up, which can benefit chemical, nucleation-based nanomaterial formations (Lin et al., 2021a, 2021b). In addition, microreactors can be used to resolve the process dynamics both in time and position along the microchannel, thus making the study of the nucleation and growth mechanism of nanocrystals feasible. Therefore, microreactor technology provides an effective way to solve the problems of large-scale continuous flow synthesis, process

control and safety of CQDs.

In the present study, NP-CQDs were prepared via a microflow method by using ethanolamine and phosphoric acid as precursors, aiming to develop a continuous and rapid method to prepare CQDs with uniform size distribution and multi-element doping. The influence of processing parameters on the structure and fluorescence properties of the products were also investigated. The demonstrated ultra-small luminescent NP-CQDs together with the simple, continuous, and controllable microflow process contributes to the development of new microreactor-based technologies for the scalable production of advanced functional nanomaterials for diverse applications.

2. Experimental

2.1 Materials

In this work, monoethanolamine (≥ 99.7 %, Sinopharm Group Chemical Co., Ltd), phosphoric acid (≥99.8 %, Sinopharm Group Chemical Co., Ltd), and ethanol (≥99.7%, Sinopharm Group Chemical Co., Ltd) were used as the raw materials. Dimethyl silicon oil (≥ 99.7%, Shanghai Titan Scientific Co., Ltd) was filled in oil bath and used as the heating medium for the microreactor. All the chemicals were used as received without further purification.

2.2 Characterization

Ultraviolet-visible (UV-Vis) absorption spectra of the prepared CQDs were collected by a TU-1950 spectrophotometer (Beijing Puxi General Instrument Co., Ltd.). The functional groups of the CQDs were analyzed by Nicolet 6700 Fourier-transform infrared spectrometer (FT-IR) (Seymour Fisher Technology Co., LTD) in the

wavelength range from 500 cm^{-1} to 4000 cm^{-1}. The surface chemical composition and bonding states of the CQDs were further examined by an X-ray photoelectron spectroscopy (XPS) using a Kratos Axis Supra DLD spectrometer equipped with an aluminum anode (Al Kα=1486.6 eV). The size and morphology of the CQDs were characterized using a transmission electron microscope (TEM, FEI Tecnai G2 F20 S-TWIN) at an accelerating voltage of 15 kV. For preparing the TEM samples, the ultrasonically treated CQDs solution was dropped on TEM grids and then dried in atmosphere for 24h. X-ray diffraction (XRD) measurements were also performed to examine the crystalline structure of the CQDs in the 2θ diffraction angle range of 15^{o} - 70^{o} , at a scanning speed of 0.5^{o} /min. The fluorescence properties of the products were analyzed by the UV-Vis spectroscopy, fluorescence spectrum and fluorescence lifetime. The photoluminescence (PL) properties of the CQDs were characterized using a CARY Eclipse spectrophotometer (Varian, USA).

2.3 Microflow CQDs synthesis

Systematic experiments were designed and carried out to study the microflow process for the synthesis of NP-CQDs, aiming to investigate the influence of the reaction time and temperature on the products. The reaction temperature was varied in the range of 110 ºC - 170 ºC, and the reaction time was within 30 min. For convenience, the prepared NP-CQDs were denoted as CQDs-x-y, where “x” is the reaction temperature, and “y” is the residence time. Specifically, CQDs-160-30 represents CQDs prepared at 160 ºC, with a reaction time of 30 min. In a typical procedure, 20 ml ethanolamine and 40 ml phosphoric acid were mixed and dissolved completely in 80

ml deionized water as the reaction solution. The solution was then transferred into a stainless-steel capillary (outer diameter=2.0 mm, inner diameter=1.0 mm) microreactor system at a fixed rate using a precision piston pump (Xingda 2PB-1040II, China) with an accuracy of 0.01 mL/min. The flow rates were set according to the residence time of the solution. The capillary was immersed in a heated oil bath, with the temperature being varied in the range of 110 ºC-170 ºC. After passing through the capillary, the solution containing NP-CQDs were collected at the outlet of the microreactor system, and then cooled down to ambient temperature. Finally, the solution was filtered by a 0.22-μm pore size nylon membrane for further characterization.

3. Results and discussion

Figure 1 shows a typical FTIR spectrum of the microflow-synthesized CQDs. The broad absorption band located at 3458cm^{-1} is indexed to the -OH stretching vibration, and the peaks at 2922cm^{-1} and 2847cm^{-1} are assigned to the stretching vibration of -NH_2 and -CH_2- functional groups, respectively (Lin et al., 2018). The peaks at 2389 cm^{-1} and 539 cm^{-1} indicate the presence of amine and phosphate, indicating that the formation of N- /P-contained functional groups as well as the good water solubility of the prepared CQDs. This is in agreement with the study of Jiang et al. (Jiang et al., 2018), where phosphorescent NP-CQDs were prepared using a microwave irradiation method. In addition, several absorption peaks were also observed at 1727 cm^{-1}, 1640cm^{-1}, 1263cm^{-1}, 1179 cm^{-1}, 1075 cm^{-1}, and 986 cm^{-1}, corresponding to the C=O, C=N, P=O, C-N/C-O , P-O-C, and P-O-H, respectively. The above absorption bands not only suggest the successful doping of N and P into the CQDs, but also reveal the generation

of the abundant functional groups on the surface of CQDs.

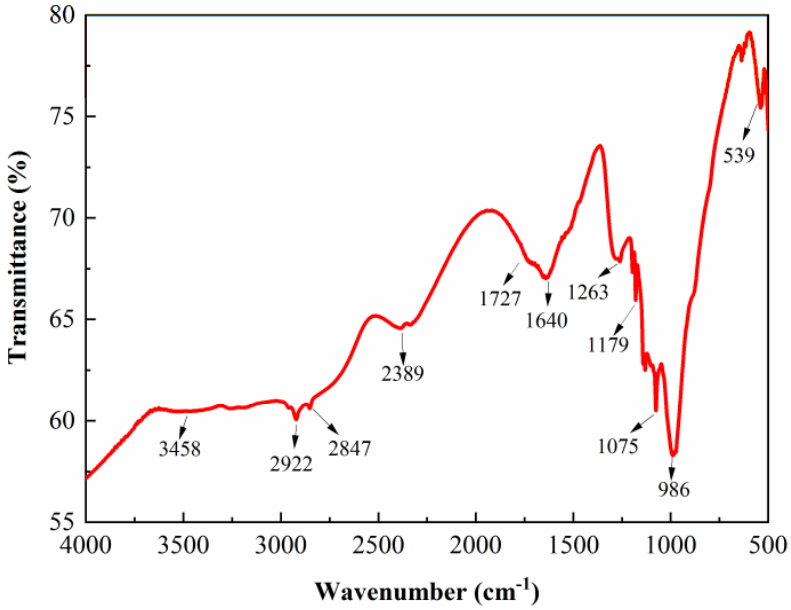

Figure 1. Representative FT-IR spectrum of the CQDs prepared by the microflow-based method.

The chemical composition and binding information of the synthesized CQDs are identified by the X-ray photoelectron spectroscopy (XPS) spectra. As shown in the full range XPS spectrum (Figure 2a), the CQDs mainly contain C, O, N, and P elements, with compositions to be 62.4%, 17.9%, 9.5%, and 10.2%, respectively. This further confirms the effective doping of N and P into the CQDs. The high-resolution spectrum of C_{1s} is given in Figure 2b, and the deconvolution of the peak indicates the presence of C-C (284.6 eV), C-N/P (285.4 eV), C-O (286.3 eV), and C=O bonds in the CDs (Figure 2b) (Lin et al., 2017). Figure 2c shows the N_{1s} bands of the synthesized CQDs. Spectral decomposition indicates the existence of three distinct components. The first peak located at 399.6 eV is assigned to the C-N=C, while the peaks at 401.1 eV and 401.8 eV are attributed to the N-$(C)_3$ and N-H bonds, respectively, in agreement with the FT-IR results (Jiang et al., 2018). The high resolution P_{2p} spectrum is deconvoluted into two peaks at 133.4 eV and 134.5 eV, attributed to the P-C and P-O bonds,

respectively (De and Karak, 2013).

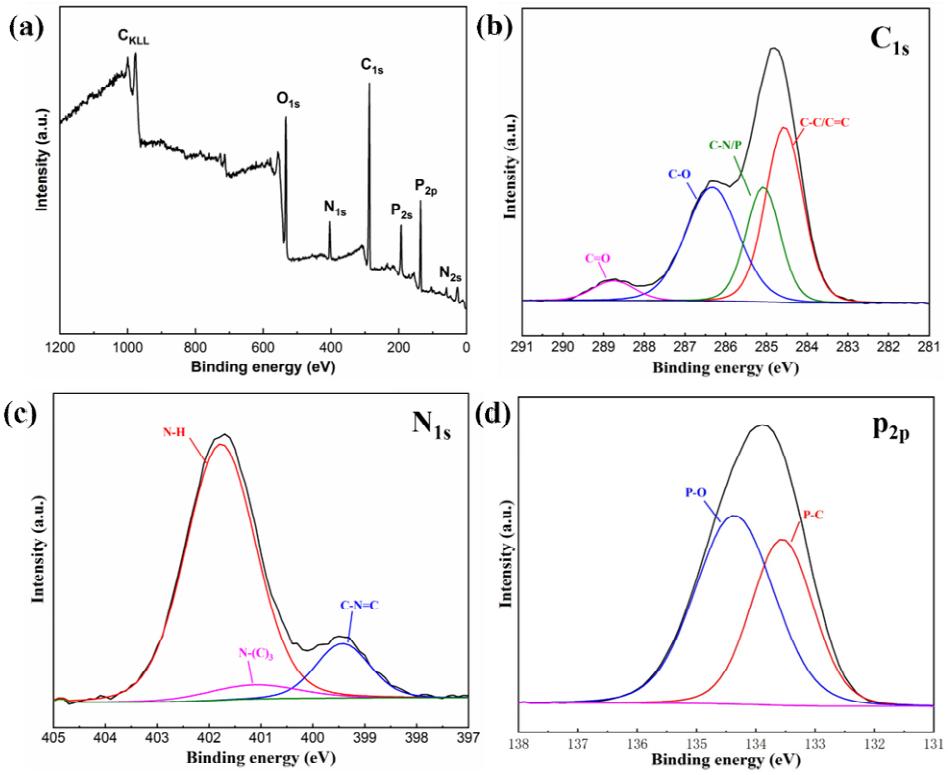

Figure 2. (a) Full XPS spectrum of the CQDs; (b) high resolution XPS spectrum of C_{1s}; (c) high-resolution XPS spectrum of N_{1s}; (d) high-resolution XPS spectrum of P_{2p}.

TEM characterization was also performed to examine the morphology and size of the microflow-prepared CQDs, as shown in Figure 3. For CQDs-140-30, it is observed that they are well dispersed, have quasi-spherical shapes and narrow size distribution (Figure 3a). The size of most of the particles is in the range of 1.0 nm - 4.0 nm, with the average size of about 2.60 nm. At higher reaction temperatures, particles tend to aggregate, and the agglomeration effect can be seen in the CQDs-160-30 sample (Figure 3c). Meanwhile, the particle size apparently increased, with an average size of 4.13 nm. In addition, the high-resolution TEM (HRTEM) micrograph further reveals the crystalline structure of the CQDs, with the lattice fringes clearly observable. The lattice spacing is measured to be 0.21 nm using Gatan Micrograph Suite ® software,

which is indexed to the (001) facet of graphite. The crystalline structure was also confirmed by the selected area electron diffraction (SAED) pattern as well as the fast Fourier transform (FFT) pattern, through the well-resolved diffraction rings and dots seen in Figure 3e.

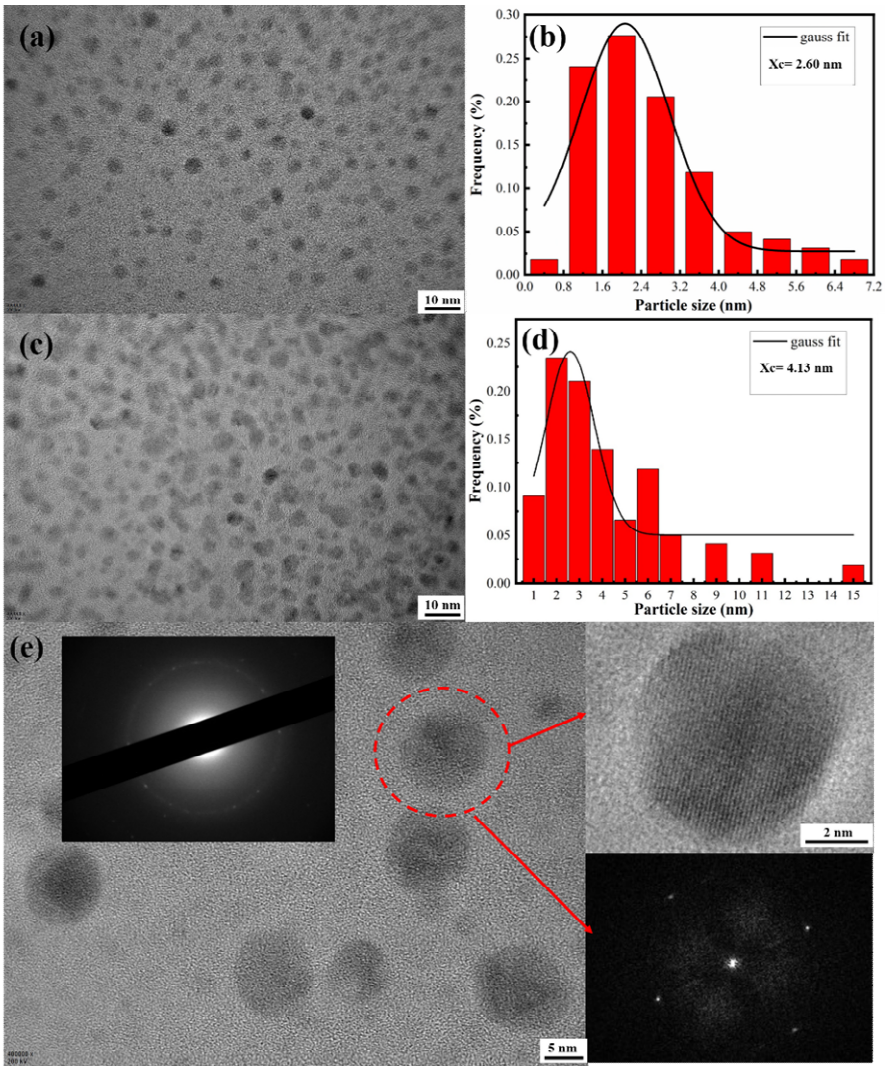

Figure 3. (a-d) TEM images and particle size distributions of the CQDs-140-30 and CQDs-160-30; (e) Magnified TEM image of the CQDs-160-30, the top-left inset is the corresponding SAED pattern, HRTEM image, and the corresponding FFT pattern on the bottom right.

Figure 4 presents the XRD pattern of the CQDs-160-30, providing additional validation for the formation of crystalline CQDs. The characteristic peaks of the carbon

dots are seen at diffraction angles of 28.5°, 40.6°, 50.3°, 58.7°, and 66.3°, corresponding to the (220), (100), (102), (103), and (104) facets, respectively. The first four facets are originated from graphitic (sp^2) carbon, while the last one is due to the diamond-like (sp^3) carbon. Same phenomena were also reported by preceding studies (Baker and Baker, 2010; Hsu et al., 2012).

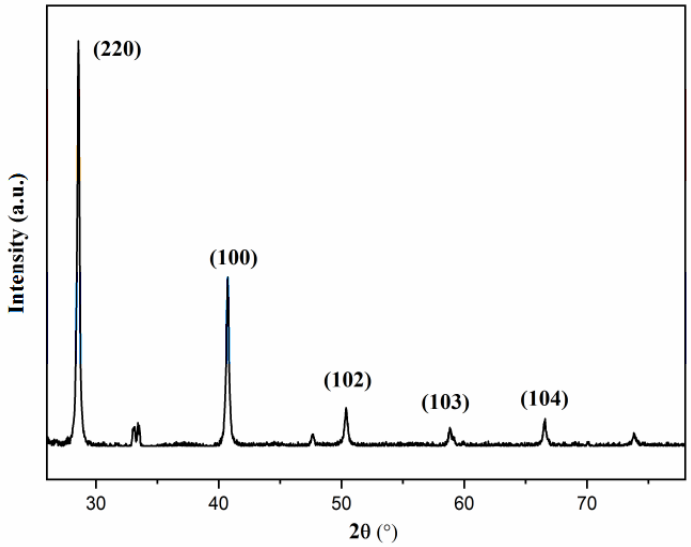

Figure 4. XRD pattern of the CQDs-160-30.

To investigate the influence of the reaction time on the synthesis of CQDs, TEM images of CQDs-140-20, CQDs-140-30, and CQDs-140-40 are shown in Figure 5. One can see that only few CQDs of quasi-spherical morphology are formed at a residence time of 20 min, with a narrow size distribution in the range of 0.5 - 2.0 nm. At prolonged reaction times, increasing numbers of CQDs are generated. Meanwhile, particles aggregate once the reaction time exceeds 30 min. It is seen that particles connect or overlap together at a residence time of 40 min. By randomly measuring 300 particles in each condition and creating the histograms of the particle size distribution, the mean particle size is found to increase from 1.15 nm at 20 min, to 2.60 nm at 30 min, and

finally reach 10.29 nm at 40 min. Therefore, to obtain well dispersed CQDs with narrow size distribution, the reaction time should be limited within 30 min.

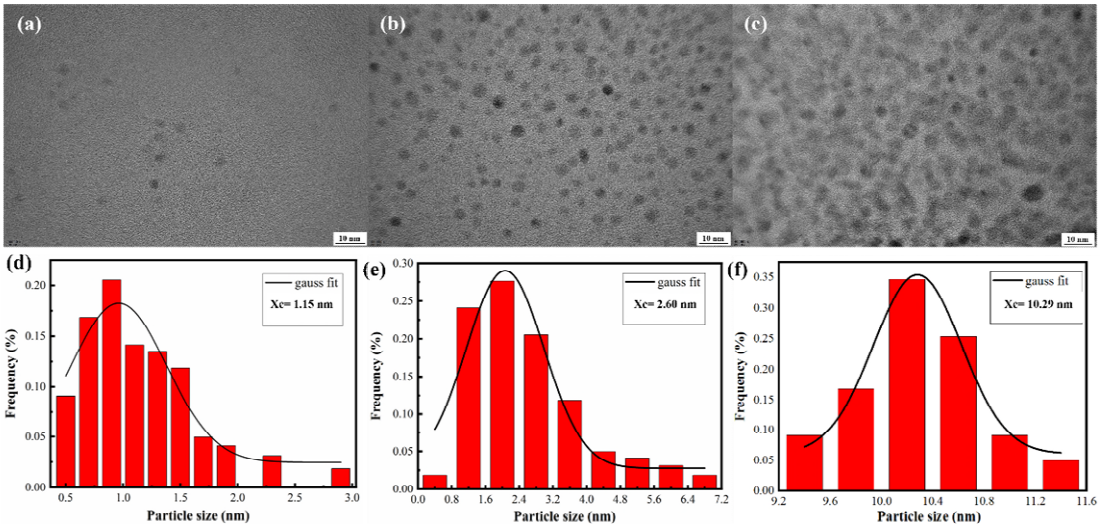

Figure 5. TEM images and particle size distributions of (a) CQDs-140-20; (b) CQDs-140-30; and (c) CQDs-140-40.

In addition to the characterization of the CQDs in terms of composition, morphology, structure, and size, their optical properties were also investigated. Figure 6 shows the UV-Vis spectra of the aqueous solution of CQDs obtained at 140 °C, with the reaction time varying from 10 min to 30 min. It can be seen that all spectra exhibit prominent peaks at ~293 nm, and have tails extending into the visible range, which corresponds to the typical n-π* transition of C=O band and the π-π* transition of conjugated C=C band (aromatic sp^2 domains) (De and Karak, 2013; Kurniawan et al., 2021). Additionally, the intensities of the UV-Vis spectra increase considerably with the reaction time, suggesting that more CQDs are formed. Indeed, loner reaction times contribute to more effective precursor conversion. Another interesting phenomenon is that a notable absorption peak was observed in the reaction solution, although the intensity was relatively weak. We repeated the detection for several times, and all the

experiments showed the same result. This can be reasonably explained by the rather slow reactions between the precursors, in which CQDs can be slowly formed due to the released heat from the acid-base neutralization reaction.

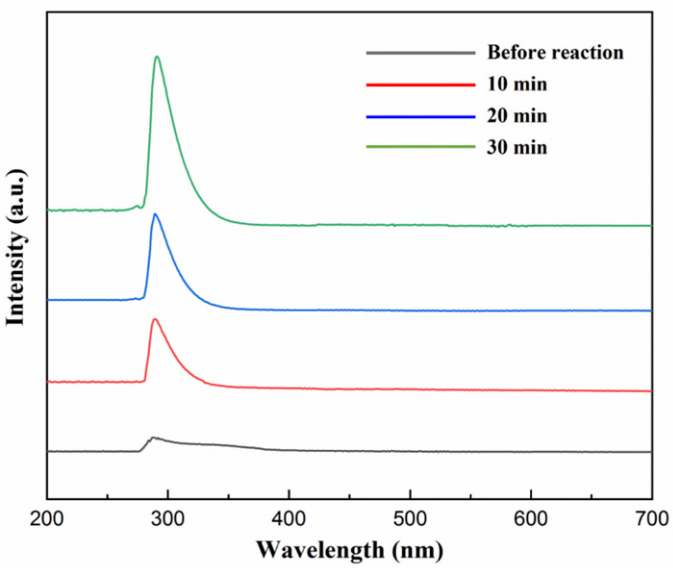

Figure 6. UV-Vis spectra of the CQDs prepared at different reaction times.

Photoluminescence (PL) is one of the most important properties of CQDs that makes them attractive for a wide range of applications. Figure 7(a) shows the 380 nm-excited PL spectra of the carbon dots obtained at different reaction times. All spectra show strong emission peaks at ~445 nm, suggesting that the as-prepared CQDs generate the photoluminescence. The intensity of the PL spectra increases considerably with the reaction time, which is due to the higher CQDs concentration in the aqueous solution. This result is in consistent with the TEM characterization, where a high amount of apparently aggregated CQDs was observed at longer reaction times.

As indicated by the Figure 7(b), the intensity of the PL emission peaks also rises significantly with the reaction temperature, especially once the temperature exceeds 150 °C. According to the previous research, the significant enhancement of PL intensity

not only caused by the formation of abundant CQDs at high temperatures, but is also closely related to the functional groups on the surface of CQDs. Phosphoric acid can act as crosslinking agent and react with ethanolamine to form polymer molecules (with C=N, C=O and other fluorescent group), leading to the much-enhanced fluorescence properties. On the other hand, it should be noted that once the reaction temperature reaches 170 °C, the capillary microreactor was easily blocked by the CQDs, which is undesirable for the synthesis process. The PL spectrum of the solution before the microflow-synthesis was also recorded, and a peak with a rather low intensity was detected at ~445 nm (inset), confirming that the precursor also produced some fluorescence emission. This result is consistent with the UV-Vis spectrum, further inferring the formation of fluorescent small molecules (containing fluorescent groups such as amino groups) via neutralization reaction.

The PL spectra of the CQDs-160-30 with variation of excitation wavelength (326-426 nm) are shown in Figure 7(c). A strong emission peak located at 421 nm was observed using an excitation wavelength of 326 nm. As the excitation shifts from 326 to 426 nm, the fluorescence wavelength of the CQDs increases from 425 to nearly 500 nm. The strong excitation-dependent photoluminescence is an important feature of CQDs (Weerasinghe et al., 2021). However, the underlying mechanism is very complex and has not yet been elucidated. A plausible explanation is that the PL behavior of CQDs is determined by the synergistic effects of the surface energy traps as well as the particle sizes. Due to the quantum confinement effects, the energy gap of CQDs increases with the decrease of the particle size. Meanwhile, the presence of various functional groups

on the surface of the CQDs may result in a series of emissive traps leading to the π-π* transition of the C-C bonds. Certain surface energy traps may dominate the emission at certain excitation wavelengths, while other surface state emissive traps may become dominant as the excitation wavelength changes, leading to the strong excitation-dependent PL behavior (De and Karak, 2013; Nguyen et al., 2015; Yu et al., 2012).

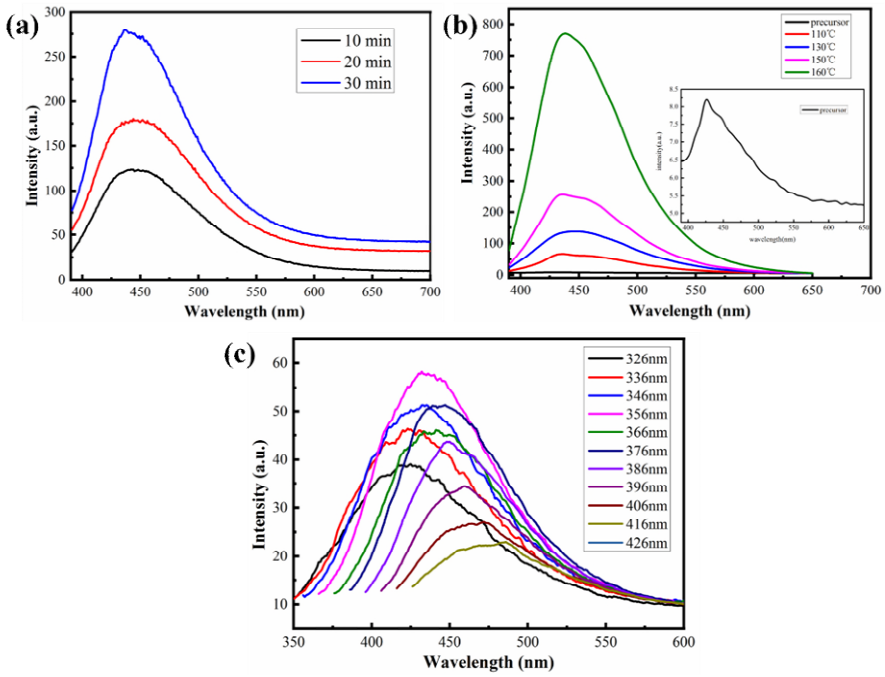

Figure 7. UV-Vis spectra of CQDs prepared at different reaction times.

It is widely accepted that the fluorescence decay curve of CQDs would show multi-exponential decay phenomenon once the CQDs have multiple emission centers (Song et al., 2015). Therefore, in this work, the fluorescence lifetimes of the microflow-synthesized CQDs were analyzed. Figure 8 shows the phosphorescence decay spectra and fitting curves (red line) of the CQDs obtained at different temperatures, with a constant reaction time of 30 min. Meanwhile, the corresponding fitting parameters of the fluorescence decay curves are listed in Table 1. The average fluorescence lifetime of CQDs is calculated using the following functions

$$I(t) = \sum B_i \, e^{(-t/\tau_i)} \quad (1)$$

$$\tau_{avg} = \sum B_i \, \tau_i^2 / \sum B_i \, \tau_i \quad (2)$$

where *I(t)* is the sum of the individual exponential decay intensities; τ_i is the decay time; B_i is the proportional coefficient of decay time (B_1 + B_2 +…+ B_i = 1); τ_{avg} is the average fluorescence lifetime. It is seen that the average fluorescence lifetime τ_{avg} of CQDs shows a decreasing trend with the increase of the reaction temperature, from 7.3762 ns at 110 °C, 6.8303 ns at 130 °C, to 5.6144 ns at 150 °C, and 5.3096 ns at 160 °C. This is due to the fact that more CQDs are generated at elevated temperatures. As a result, the associated aggregation of CQDs as well as the cross-linked polymers formed on the surface of the CQDs will lead to the quenching of fluorescence (Qu et al., 2012). Therefore, to prepare CQDs with the long fluorescence lifetimes, the agglomeration of CQDs should be reduced, e.g., by operating at low temperatures or maintaining short residence times.

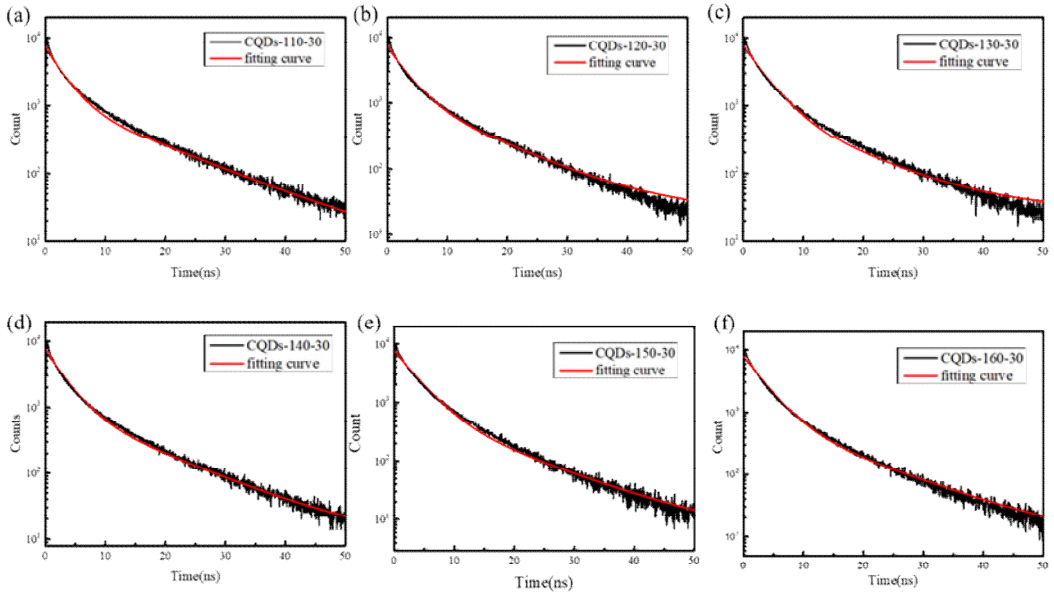

Figure 8. Phosphorescence decay spectra and fitting curves (red line) of (a) CQDs-110-30; (b) CQDs-

120-30; (c) CQDs-130-30; (d) CQDs-140-30; (e) CQDs-150-30; (f) CQDs-160-30.

Table 1. Fitting parameters of fluorescence decay curves at different temperatures

Temperature /°C	110	130	150	160
τ_1/ns	0.7158	0.9989	0.1756	1.2067
B_1	4374.49	4715.32	1366.237	4413.181
τ_2/ns	3.3494	3.8921	1.4488	3.7421
B_2	3838.036	4220.216	4234.859	3944.601
τ_3/ns	11.8937	12.9520	4.2034	11.1064
B_3	1351.588	955.115	3337.237	988.236
τ_4/ns	—	—	10.3154	—
B_4	—	—	962.150	—
τ_{avg}/ns	7.3762	6.8303	5.6144	5.3096
χ^2	1.169	1.220	1.147	1.105

Furthermore, the fluorescence lifetimes of CQDs prepared at different residence times were also studied. The relevant PL decay spectra and fitting curves (red line) are shown in Figure 9, with the fitting parameters being listed in Table 2. One can see that the average fluorescence lifetimes of CQDs synthesized show a decreasing trend, from 6.013 ns at 10 min, to 5.8608 ns at 20 min, and finally became 5.3096 ns at 30 min. This is also due to the aggregation of CQDs at longer reaction times, which would cause fluorescence quenching.

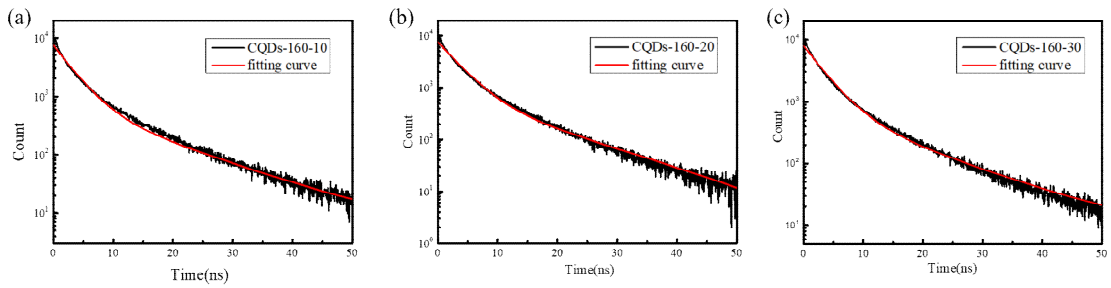

Figure 9. PL decay spectra and fitting curves (red line) of (a) CQDs-160-10; (b) CQDs-160-20; (c)

CQDs-160-30

Table 2. Fitting parameters of the PL decay curves at different residence times

Residence times /min	τ_1/ns	B_1	τ_2/ns	B_2	τ_3/ns	B_3	τ_{avg}/ns	χ^2
10	0.8823	4661.734	3.5393	3977.108	11.2546	947.981	6.0130	1.176
20	1.1432	4547.730	3.7018	3943.970	10.1122	1023.243	5.8608	1.041
30	1.2067	4413.181	3.7421	3944.601	11.1064	988.236	5.3096	1.105

4. Conclusion

The luorescent phosphorus and nitrogen co-doped carbon quantum dots (NP-CQDs) have been prepared by a continuous microflow-based approach, using the customized microchannel reactors and process chemistry. The structure, composition and fluorescence performance of the products were investigated by FTIR, XPS, TEM, XDR, as well as the optical analysis methods. The results indicate that crystalline NP-CQDs with small size and narrow size distribution have been generated. Moreover, the N and P elements were effectively doped into the CQDs. These doped elements formed the abundant functional groups (e.g. C-N/P, C=N, P=O, C-O , -NH_2, P-O-C, etc.) on the surface of CQDs, further endowing them with new functionalities as well as the improved photoluminescence properties. With an increase of the reaction time or the temperature, the particle sizes also increase. Meanwhile, particle agglomeration could be observed at reaction temperatures above 150 °C. However, once the temperature exceeds 160 °C, the capillary microreactor can be blocked by the aggregated COQs.

Optical characterization was used to examine the CQDs fluorescence performance, and revealed that the PL intensity is closely related to the processing parameters. With

the rise of the temperature or the reaction time, a larger amount of CQDs is produced, leading to a significant increase of the fluorescence emission intensity. On the other hand, the aggregation of CQDs may cause fluorescence quenching, resulting in a decrease of the fluorescence lifetimes. In addition, the CQDs exhibit the excitation wavelength-dependent photoluminescence, which may be caused by different emission centers originated from the functional groups on the CQDs surface. Different emission centers generate emission at certain wavelengths under the excitation at a particular wavelength.

Collectively, these findings offer a simple and effective approach for the rapid and continuous synthesis of doped/co-doped fluorescent carbon quantum dots, making them attractive for various applications in diverse fields from biotechnology and medicine to energy conversion and environmental monitoring. The demonstrated ability for doping and functionalizing CDQs contributes to the development of advanced continuous, scalable, industry-relevant flow chemistry processes and precisely engineered products.

Acknowledgements

The authors greatly appreciate the funding support from Natural Science Foundation of Jiangsu Province (BK20190605), National Natural Science Foundation of China (52004102, 22078125), Postdoctoral Science Foundation of China (2021M690068), the Fundamental Research Funds for the Central Universities (JUSRP221018), Key Laboratory of Nanodevices of Jiangsu Province (21SZ02). This work was partially supported by the Australian Research Council and QUT Centre for Materials Science.

Reference

Baker, S.N., Baker, G.A., 2010. Luminescent carbon nanodots: Emergent nanolights. Angew. Chemie - Int. Ed. 49, 6726–6744. https://doi.org/10.1002/anie.200906623

Castro, H.P.S., Souza, V.S., Scholten, J.D., Dias, J.H., Fernandes, J.A., Rodembusch, F.S., Dos Reis, R., Dupont, J., Teixeira, S.R., Correia, R.R.B., 2016. Synthesis and Characterisation of Fluorescent Carbon Nanodots Produced in Ionic Liquids by Laser Ablation. Chem. - A Eur. J. 22, 138–143. https://doi.org/10.1002/chem.201503286

De, B., Karak, N., 2013. A green and facile approach for the synthesis of water soluble fluorescent carbon dots from banana juice. RSC Adv. 3, 8286–8290. https://doi.org/10.1039/c3ra00088e

El-Shabasy, R.M., Elsadek, M.F., Ahmed, B.M., Farahat, M.F., Mosleh, K.M., Taher, M.M., 2021. Recent developments in carbon quantum dots: Properties, fabrication techniques, and bio-applications. Processes 9, 388. https://doi.org/10.3390/pr9020388

Hsu, P.C., Shih, Z.Y., Lee, C.H., Chang, H.T., 2012. Synthesis and analytical applications of photoluminescent carbon nanodots. Green Chem. 14, 917–920. https://doi.org/10.1039/c2gc16451e

Jiang, K., Wang, Y., Gao, X., Cai, C., Lin, H., 2018. Facile, Quick, and Gram-Scale Synthesis of Ultralong-Lifetime Room-Temperature-Phosphorescent Carbon Dots by Microwave Irradiation. Angew. Chemie - Int. Ed. 57, 6216–6220. https://doi.org/10.1002/anie.201802441

Kurniawan, D., Jhang, R., Ostrikov, K.K., Chiang, W., 2021. Microplasma-Tunable Graphene Quantum Dots for Ultrasensitive and Selective Detection of Cancer and Neurotransmitter Biomarkers. ACS Appl. Mater. Interfaces 13, 34572–34583.

Li, J., Yun, X., Hu, Z., Xi, L., Li, N., Tang, H., Lu, P., Zhu, Y., 2019. Three-dimensional nitrogen and phosphorus co-doped carbon quantum dots/reduced graphene oxide composite aerogels with a hierarchical porous structure as superior electrode materials for supercapacitors. J. Mater. Chem. A 7, 26311–26325. https://doi.org/10.1039/c9ta08151h

Lin, L., Quoc Pho, H., Zong, L., Li, S., Pourali, N., Rebrov, E., Nghiep Tran, N., Ostrikov, K. (Ken),

Hessel, V., 2021a. Microfluidic plasmas: Novel technique for chemistry and chemical engineering. Chem. Eng. J. 417, 129355. https://doi.org/10.1016/j.cej.2021.129355

Lin, L., Starostin, S.A., Li, S., Khan, S.A., Hessel, V., 2018. Synthesis of yttrium oxide nanoparticles via a facile microplasma-assisted process. Chem. Eng. Sci. 178, 157–166. https://doi.org/10.1016/j.ces.2017.12.041

Lin, L., Starostin, S.A., Ma, X., Li, S., Khan, S.A., Hessel, V., 2019. Facile synthesis of lanthanide doped yttria nanophosphors by a simple microplasma-assisted process. React. Chem. Eng. 4, 891–898. https://doi.org/10.1039/c8re00357b

Lin, L., Starostin, S.A., Wang, Q., Hessel, V., 2017. An atmospheric pressure microplasma process for continuous synthesis of titanium nitride nanoparticles. Chem. Eng. J. 321, 447–457. https://doi.org/10.1016/j.cej.2017.03.128

Lin, L., Yin, Y., Starostin, S.A., Xu, H., Li, C., Wu, K., He, C., Hessel, V., 2021b. Microfluidic fabrication of fluorescent nanomaterials : A review. Chem. Eng. J. 425, 131511.

Ling, L., Zhu, Z., Shen, H., Cheng, R., Ye, H.G., Li, Q., Wang, C.F., Chen, S., 2020. One-Step Facile Synthesis of Fluorescent Carbon Dots via Magnetic Hyperthermia Method. Ind. Eng. Chem. Res. 59, 4968–4976. https://doi.org/10.1021/acs.iecr.9b06833

Ma, X., Li, S., Hessel, V., Lin, L., Meskers, S., Gallucci, F., 2020. Synthesis of N-doped carbon dots via a microplasma process. Chem. Eng. Sci. 220, 115648. https://doi.org/10.1016/j.ces.2020.115648

Ma, X., Li, S., Hessel, V., Lin, L., Meskers, S., Gallucci, F., 2019. Synthesis of luminescent carbon quantum dots by microplasma process. Chem. Eng. Process. - Process Intensif. 140, 29–35. https://doi.org/10.1016/j.cep.2019.04.017

Nguyen, V., Si, J., Yan, L., Hou, X., 2015. Electron-hole recombination dynamics in carbon nanodots. Carbon N. Y. 95, 659–663. https://doi.org/10.1016/j.carbon.2015.08.066

Park, Y., Yoo, J., Lim, B., Kwon, W., Rhee, S.W., 2016. Improving the functionality of carbon nanodots: Doping and surface functionalization. J. Mater. Chem. A 4, 11582–11603. https://doi.org/10.1039/c6ta04813g

Qu, J., Zhang, X., Liu, Y., Xie, Y., Cai, J., Zha, G., Jing, S., 2020. N, P-co-doped carbon dots as a dual-mode colorimetric/ratiometric fluorescent sensor for formaldehyde and cell imaging via an aminal reaction-induced aggregation process. Microchim. Acta 187, 355. https://doi.org/10.1007/s00604-020-04337-0

Qu, S., Wang, X., Lu, Q., Liu, X., Wang, L., 2012. A Biocompatible Fluorescent Ink Based on Water-Soluble Luminescent Carbon Nanodots. Angew. Chemie 124, 12381–12384. https://doi.org/10.1002/ange.201206791

Song, Y., Zhu, S., Zhang, S., Fu, Y., Wang, L., Zhao, X., Yang, B., 2015. Investigation from chemical structure to photoluminescent mechanism: A type of carbon dots from the pyrolysis of citric acid and an amine. J. Mater. Chem. C 3, 5976–5984. https://doi.org/10.1039/c5tc00813a

Weerasinghe, J., Scott, J., Deshan, A.D.K., Chen, D., Singh, A., Sen, S., Sonar, P., Vasilev, K., Li, Q., Ostrikov, K.K., 2021. Monochromatic Blue and Switchable Blue-Green Carbon Quantum Dots by Room-Temperature Air Plasma Processing. Adv. Mater. Technol. 2100586. https://doi.org/10.1002/admt.202100586

Yu, P., Wen, X., Toh, Y.R., Tang, J., 2012. Temperature-dependent fluorescence in carbon dots. J. Phys. Chem. C 116, 25552–25557. https://doi.org/10.1021/jp307308z